Multiple-gap structure in electric-field-induced surface superconductivity

Yousuke Mizohata, Masanori Ichioka,* and Kazushige Machida
Department of Physics, Okayama University, Okayama 700-8530, Japan
(Received 9 November 2012; revised manuscript received 21 December 2012; published 11 January 2013)

Local superconducting gap structure is studied as a function of nanoscale depth in electric-field-induced surface superconductivity such as in $SrTiO_3$. We examine solutions of the Bogoliubov–de Gennes equation in two limiting confinement potential cases of an electric field with and without screening effects. As unique properties different from bulk superconductivity, there appear in-gap states even for isotropic s-wave pairing, due to the multiple-gap structure of sub-band-dependent surface superconductivity. These determine the depth dependence of local superconductivity.

DOI: 10.1103/PhysRevB.87.014505 PACS number(s): 74.78.−w, 73.20.At, 74.20.Pq, 74.81.−g

I. INTRODUCTION

The electric-field-induced carrier-doping technique, using a field-effect transistor structure or an electric double-layer transistor structure,[1–5] has attracted much attention as a new method of carrier doping, apart from the methods of chemical doping. A merit of electric-field-induced doping is that we can control the doping carrier density by the gate voltage in the same sample. This will be a powerful platform in future studies of condensed matter physics. When this is used at the surface of insulators, carriers are induced near the surface and trapped in the confinement potential of the electric field. Using a strong enough field by electric double-layer transistor, we can realize superconductivity of the surface metallic states at low temperatures T, such as in $SrTiO_3$,[1] ZrNCl,[2] $KTaO_3$,[3] and MoS_2.[4,5] Gate voltage control of surface superconductivity in $SrTiO_3$ was also realized at the interface of $LaTiO_3/SrTiO_3$ and $LaAlO_3/SrTiO_3$.[6,7]

Compared to these developments in experimental research, theoretical understanding is not enough for properties of the electric-field-induced surface superconductivity. We must discuss whether the surface superconductivity has the same properties as the bulk superconductivity or whether it has different unique properties. In future experiments on unconventional superconductivity produced on a surface, we have to distinguish unique properties of surface superconductivity and exotic properties of unconventional superconductivity.

As different properties from bulk metallic states, sub-bands are formed in the surface metallic states due to the confinement potential by strong electric fields.[1] Since multiple sub-bands are occupied by surface carriers, this system is not an ideal two-dimensional state. We also note that the local carrier density $n(z)$ shows spatial variation as a function of depth z from the surface in surface metallic states, while $n(z)$ is constant in bulk metallic states. Quantitative estimatation of the z dependence is one of the problems for the electric-field-induced metallic state. Therefore, also in theoretical studies of surface superconductivity, we need to know the detailed spatial structure of the superconducting gap on the nanoscale and its sub-band dependence. These studies will enable us to find differences from bulk superconductivity.

In this paper, we study unique properties: local electronic states and sub-band dependence in electric-field-induced superconductors. We discuss the multiple-gap structure of the sub-band-dependent surface superconductivity. Since we determine the spatial structure of the order of the Thomas-Fermi length near the surface, we solve the Bogoliubov–de Gennes (BdG) equation[8] under an electric field $F(z)$. We discuss the depth z dependence perpendicular to the surface at $z = 0$. As for the confinement potential $V(z)$ by $F(z)$, we compare two cases: the triangular potential and the self-consistent potential.[9,10] The latter is the case where induced carriers completely screen the applied electric field. The former is the opposite limit, where screening is negligible.

This paper is organized as follows. After we explain our theoretical formulation of the BdG equation under electric fields in Sec. II, we study the depth dependence of the local superconducting gap structure in Sec. III and the gap structure of the sub-band modes in the spectral weight in Sec. IV. In order to discuss the relationship of the sub-band-dependent gap structure and the depth dependence of superconducting states, we perform analyses of sub-band decomposition for surface superconductivity in Sec. V. The last section is devoted to a discussion and summary, including the topics of Bardeen-Cooper-Schrieffer (BCS)–Bose-Einstein condensation (BEC) crossover phenomena in surface superconductivity.

II. BOGOLIUBOV–DE GENNES THEORY IN CONFINEMENT BY AN ELECTRIC FIELD

Throughout this paper, the energy, length, and local carrier density, respectively, are presented in units of eV, nm, and nm^{-3}. We typically consider the case of a sheet carrier density $n_{2D} = 6.5 \times 10^{13}$ cm^{-2}, and the electric field at the surface is given by $F_0 \equiv F(z = 0) = 1.4 \times 10^{-3}$ V/nm. The triangular potential with this F_0 corresponds to one of the cases calculated in Ref. 1 for $SrTiO_3$, while a single-band case of effective mass $m^* = 4.8m_0$ is considered here. m_0 is the free electron mass.

In the normal state,[1,9] the eigenenergy E_ϵ and wave function $u_\epsilon(\mathbf{r}) = e^{i(k_x x + k_y y)} u_\epsilon(z)/\sqrt{S}$ are determined by the Schrödinger equation

$$K u_\epsilon(z) = E_\epsilon u_\epsilon(z), \tag{1}$$

with

$$K = -\frac{\hbar^2}{2m^*}\frac{d^2}{dz^2} + E_\parallel + V(z) - \mu, \tag{2}$$

$E_\parallel = \hbar^2 k_\parallel^2/2m^*$, $k_\parallel^2 = k_x^2 + k_y^2$, and S the unit area of surface. We assume that the wave functions vanish at $z = 0$ as the boundary condition. In the direction parallel to the surface, the eigenstates are given by wave numbers k_x and k_y of plane waves. Thus, the eigenstates of Eq. (1) are labeled by $\epsilon \equiv (k_x, k_y, \epsilon_z)$. ϵ_z is the label for sub-bands coming from quantization by confinement in the z direction. The local carrier density is calculated as $n(z) = 2n_\uparrow(z)$ with

$$n_\uparrow(z) = \sum_\epsilon |u_\epsilon(z)|^2 f(E_\epsilon), \tag{3}$$

where $f(E)$ is the Fermi distribution function. To fix n_{2D}, we tune the chemical potential μ. In the triangular potential case, the confinement potential is given by $V(z) = |e|F_0 z$. For the self-consistent potential,

$$F(z) = F_0 \left(1 - \int_0^z n(z')dz'/n_{2D}\right), \tag{4}$$

by Gauss's law, considering the screening by $n(z)$, and

$$V(z) = |e| \int_0^z F(z')dz'. \tag{5}$$

As $F(z \to \infty) = 0$, $n_{2D} = \int_0^\infty n(z')dz'$. Iterating calculations of Eqs. (1) and (2) and Eqs. (3)–(5) in the region $0 \leqslant z \leqslant L$, we determine $V(z)$ in the case of the self-consistent potential. Typically we use $L = 80$ nm.

In the superconducting state, the wave function

$$\begin{pmatrix} u_\epsilon(\mathbf{r}) \\ v_\epsilon(\mathbf{r}) \end{pmatrix} = \frac{1}{\sqrt{S}} e^{i(k_x x + k_y y)} \begin{pmatrix} u_\epsilon(z) \\ v_\epsilon(z) \end{pmatrix} \tag{6}$$

is determined by solving the BdG equation[8,11,12]

$$\begin{pmatrix} K & \Delta(z) \\ \Delta(z) & -K \end{pmatrix} \begin{pmatrix} u_\epsilon(z) \\ v_\epsilon(z) \end{pmatrix} = E_\epsilon \begin{pmatrix} u_\epsilon(z) \\ v_\epsilon(z) \end{pmatrix}. \tag{7}$$

The pair potential $\Delta(z)$ is self-consistently calculated by

$$\Delta(z) = V_{\text{pair}} \sum_\epsilon u_\epsilon(z) v_\epsilon(z) f(-E_\epsilon) \tag{8}$$

with the energy cutoff E_{cut} of the pairing interaction. Here, we consider a conventional case of isotropic s-wave pairing. We typically use $V_{\text{pair}} = 0.04$, $E_{\text{cut}} = 0.01$, and $T \sim 0$.

III. DEPTH DEPENDENCE OF LOCAL SUPERCONDUCTING GAP STRUCTURE

First, we study the local density of states (LDOS) $N(E,z) = 2N_\uparrow(E,z)$ with[11,12]

$$N_\uparrow(E,z) = \sum_{\epsilon=(k_x,k_y,\epsilon_z)} |u_\epsilon(z)|^2 \delta(E - E_\epsilon). \tag{9}$$

The left panel in Fig. 1(a) presents $N(E,z)$ for the triangular potential. There, we see steps of LDOS by the sub-band structure of quantized bound states, as in the normal state.[1] The lowest sub-band appears at $E > E_{l=1,\min} \sim 0.0059$ near the surface. The continuum distribution above $E_{l=1,\min}$ comes from finite $E_\parallel \geqslant 0$. Similarly, the LDOS of the second sub-band appears at $E > E_{l=2,\min} \sim 0.0103$, and the LDOS of the third sub-band at $E > E_{l=3,\min} \sim 0.0138$. Their contributions overlap each other at higher energies. When the sub-band

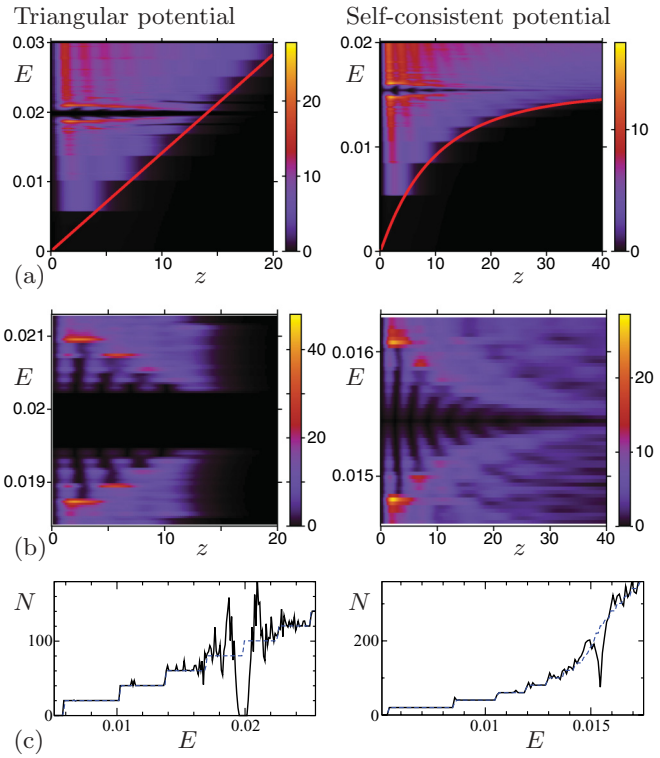

FIG. 1. (Color online) (a) Density plot of LDOS $N(E,z)$ as a function of z and $E + \mu$. The solid line presents the confinement potential $V(z)$. (b) The LDOS $N(E,z)$ in (a) is focused near the superconducting gap. (c) DOS $N(E)$ as a function of $E + \mu$. Dashed lines present $N(E)$ for the normal state. Left: Triangular potential. Right: Self-consistent potential.

level l is higher, the eigenenergy $E_{l,\min}$ becomes higher, and the distribution spreads to a deeper z from the surface. The superconducting gap appears near $\mu \sim 0.0198$.

The $N(E,z)$ for the self-consistent potential is presented in the right panel in Fig. 1(a). There, we see step structures of sub-bands in the low-energy region, but the step size becomes smaller at higher energies, because the slope of $V(z)$ decreases to 0 as a function of z by the screening effect. Since the chemical potential is located at $\mu \sim V(z \to \infty) \sim 0.0154$, occupied states with $E < \mu$ are bound states, and empty states with $E > \mu$ are scattering states which are free of the confinement potential. The superconducting gap opens between the bound states and the scattering states.

The superconducting gap structures are shown in Fig. 1(b). Even in the isotropic s-wave pairing, we see in-gap states which have oscillations as a function of z and steps of gap edges as a function of E as characteristic features of electric-field-induced surface superconductivity. High-intensity peaks of $N(E,z)$ correspond to the maximum gap edge, whose gap amplitude decreases discontinuously with increasing z. In the self-consistent potential (right panel), it reduces to 0 at large z.

Figure 1(c) shows the density of states (DOS) $N(E)$ after z integration of $N(E,z)$. Because of the in-gap states, the gap structure in $N(E)$ is different from that of bulk isotropic s-wave superconductors. In the triangular potential (left panel), the gap edge has a width from the minimum gap to the gap-edge peak of the maximum gap, as in anisotropic s-wave

superconductors. In the self-consistent potential (right panel), a full-gap structure does not exist, since low-energy states exist until near μ. The gap shape is similar to that of anisotropic superconductors with gap nodes.

IV. GAP STRUCTURE OF THE SUB-BAND MODE IN SPECTRAL WEIGHT

We discuss that these superconducting gap structures come from the sub-band dependence of superconductivity. For the sub-band decomposition, we calculate the spectral weight $N(E,k_\parallel,z) = 2N_\uparrow(E,k_\parallel,z)$ given by

$$N_\uparrow(E,k_\parallel,z) = \sum_{\epsilon_z} |u_\epsilon(z)|^2 \delta(E - E_\epsilon) \tag{10}$$

from $N_\uparrow(E,k_\parallel,z) = -\pi^{-1}\mathrm{Im}G_\uparrow(E,k_\parallel,z)$ with Green's function

$$G_\uparrow(E,k_\parallel,z) = \int e^{-\mathrm{i}(k_x\tilde{x}+k_y\tilde{y})} G_\uparrow(E,\mathbf{r},\mathbf{r}')d\tilde{x}d\tilde{y}|_{z=z'}, \tag{11}$$

$$G_\uparrow(E,\mathbf{r},\mathbf{r}') = \sum_\epsilon \frac{u_\epsilon^*(\mathbf{r})u_\epsilon(\mathbf{r}')}{E + \mathrm{i}0 - E_\epsilon}, \tag{12}$$

and $(\tilde{x},\tilde{y}) \equiv (x - x', y - y')$.[13] The z integration of $N(E,k_\parallel,z)$ is given by $N(E,k_\parallel) = \int_0^L N(E,k_\parallel,z)dz$. In Fig. 2 we show $N(E,k_\parallel)$, which appear at eigenenergies E_ϵ. There we see multiple parallel lines of the dispersion relation as a function of $E_\parallel$, corresponding to sub-bands of surface bound states. From the bottom, the lines are assigned to sub-band level $l = 1, 2, \ldots,$ as indicated in Fig. 2. In the case of the self-consistent potential, the energy distance of the dispersion relation between sub-bands decreases for higher sub-bands, and the spectral weight becomes continuous near $E_\parallel \sim 0$ at $E > \mu$ in the scattering state.

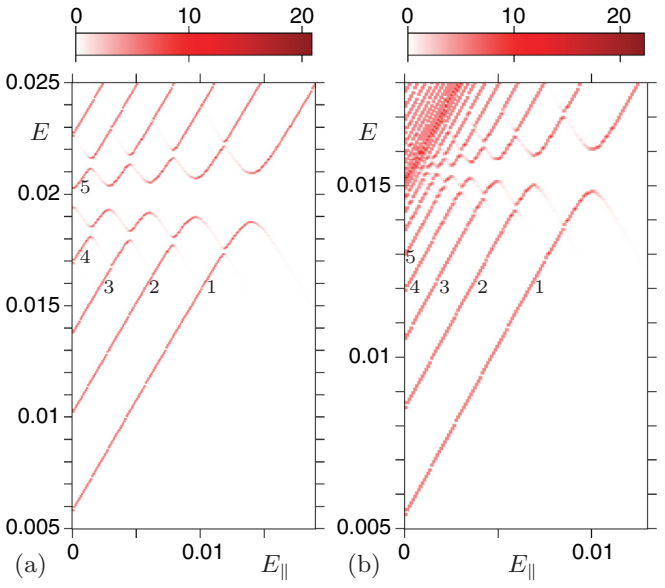

FIG. 2. (Color online) Density plot of spectral weight $N(E,k_\parallel)$ as a function of $E_\parallel = \hbar^2 k_\parallel^2/2m^*$ and $E + \mu$ for (a) the triangular potential and (b) the self-consistent potential. Numbers 1–5 indicate the sub-band level l.

In the superconducting state, gaps open at crossing points of the particle mode and the inverted hole mode at $E = \mu$, forming Bogoliubov's dispersion relations of superconductivity for each level of sub-band. The superconducting gap is larger for lower sub-bands, indicating the multiple-gap structure of surface superconductivity. In the case of the triangular potential, the occupied lower sub-bands have different but finite gaps. In the case of the self-consistent potential, sub-bands are occupied until quite higher levels, where the superconducting gap decreases to 0. Therefore, the in-gap states appear until near $E = \mu$. As for the z dependence of the spectral weight $N(E,k_\parallel,z)$, the contribution of the lower sub-band is dominant near the surface. The contributions of higher sub-bands become dominant at deeper z.

V. SUB-BAND DECOMPOSITION OF LOCAL SUPERCONDUCTING STATES

In Fig. 3(a), we present the local carrier density $n(z)$ and the sub-band decomposition. The eigenstates of the dispersion relations in Fig. 2 are classified to each sub-band level l. In the lth sub-band, the wave function of the form of Airy functions has $l - 1$ nodes along the z direction.[1] The higher sub-band contributions can penetrate into deeper z. Since the LDOS is integrated over $E_{l,\min} < E < \mu$ to obtain $n(z)$, lower sub-band contributions to $n(z)$ becomes larger, because of the smaller $E_{l,\min}$. The pair potential $\Delta(z)$ and the sub-band decomposition in Fig. 3(b) have a spatial structure similar to those of $n(z)$. It is noted that the sub-band-dependent pair potential becomes lower for higher sub-bands. In the self-consistent potential (right panels), while the lower sub-band contributions are dominant, $n(z)$ and $\Delta(z)$ include contributions from further higher sub-band levels $l > 5$. Therefore, tails of $n(z)$ and $\Delta(z)$ survive until deeper z.

To discuss the origin of the superconducting gap structure in Fig. 1, sub-band decompositions of the LDOS are presented in Fig. 4. From Fig. 4(a), we see that the lowest sub-band contribution ($l = 1$) to $N(E,z)$ has a large constant superconducting gap, but its distribution is restricted to very

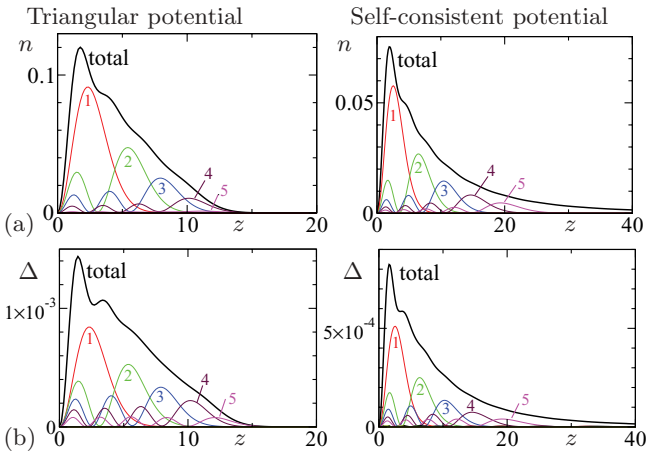

FIG. 3. (Color online) (a) Local carrier density $n(z)$ and (b) superconducting pair potential $\Delta(z)$ as a function of z. Sub-band decompositions are also presented for sub-band levels $l = 1, \ldots, 5$. Left: Triangular potential. Right: Self-consistent potential.

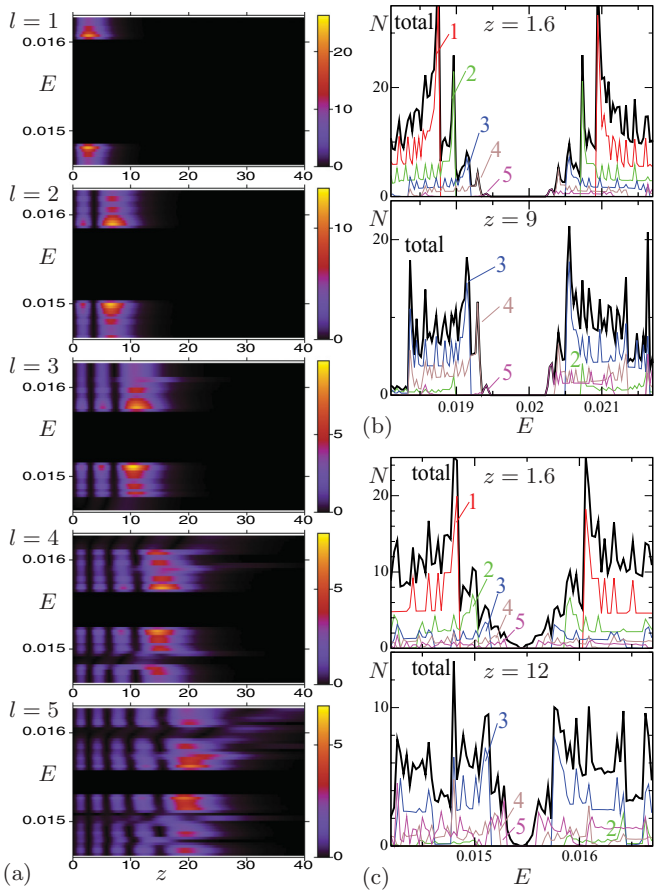

FIG. 4. (Color online) (a) Density plot of sub-band decomposition of LDOS as a function of z and $E+\mu$ for sub-band levels $l = 1,2,\ldots,5$ in the case of the self-consistent potential. (b) LDOS $N(E,z)$ and sub-band decomposition at $z = 1.6$ and 9 in the case of the triangular potential. (c) The same as (b), but at $z = 1.6$ and 12 in the case of the self-consistent potential.

near the surface. The contributions from higher sub-bands, $l = 2, 3, \ldots$, have a smaller constant gap, and the distributions spread until deeper z. By the combination of these sub-band contributions, the in-gap states and the z dependence of superconducting gap structure in Fig. 1 are created. These sub-band contributions are clear also in the LDOS spectra in Figs. 4(b) and 4(c). There, we see multiple peaks of gap edge from sub-band contributions. Near the surface ($z = 1.6$), all sub-band contributions appear, and lower sub-band contributions are dominant. Therefore the main peak corresponds to the gap edge of the largest gap by the lowest sub-band. In the lower panels in Figs. 4(b) and 4(c) for deeper z, since lower sub-band contributions ($l = 1$ and 2) vanish, the main peak of the gap edge appears at a lower gap energy corresponding to higher sub-band ($l = 3$) contributions.

In addition to the superconducting gap at $E = \mu$, extra small gaps appear at energies outside the superconducting gap, as shown in Fig. 2. This occurs by crossing of the hole and particle modes between different sub-bands. We see these extra gaps in higher sub-band contributions also in Fig. 4(a). Because of the extra gaps, the LDOS in Figs. 4(b) and 4(c) has many extra peaks outside of the main gap energy.

We note that low-energy in-gap electronic states are not determined locally by $\Delta(z)$ in the length order of nanoscale in this system. This is contrasted with the conventional case where $\Delta(z)$ is suppressed on the length scale of the superconducting coherence length.[14–17] There low-energy states appear as localized states by suppression of the local gap. In the system of electric-field-induced surface superconductivity, approaching $z \to 0$ near the surface, $\Delta(z)$ is suppressed toward 0 in the length scale of the order of nanometers, as shown in Fig. 3(a). However, in Fig. 4(a), we see that localized low-energy in-gap states do not appear in the surface region ($z < 2$) of suppressed $\Delta(z)$. The local state of the lowest sub-band has a uniform gap with the highest gap amplitude [top panel in Fig. 4(a)]. This indicates that the in-gap states reported in this paper are not due to the suppression $\Delta(z \to 0) \to 0$. Rather, the in-gap states come from the deeper region, as tails of wave functions for higher sub-band levels in Fig. 4(a). This is one of the intrinsic features of electric-field-induced superconductivity.

VI. DISCUSSION AND SUMMARY

As future experiments to confirm the in-gap states due to the characteristic multiple-gap structure, we expect observations of LDOS such as by point-contact tunneling spectroscopy, which will visualize the gap structures in the upper panels of Figs. 4(b) and 4(c). The contributions of the in-gap states will be observed in experiments sensitive to the DOS of the superconducting gap structure, such as magnetic resonance and optical absorptions. Electric-field-induced doping will be an important platform to study unconventional superconductivity. Before that, it is important to clarify the difference in properties of surface superconductivity versus bulk superconductivity in conventional superconductors, as suggested in this work. As a concept of multiple-gap structure, electric-field-induced surface superconductivity can be said to be a new type of multiband superconductor. We will see some behaviors similar to those of multiband superconductors such as MgB_2- and Fe-based superconductors. The number of contributing sub-bands can be controlled by the gate voltage.

We point out the interesting possibility of realizing the BCS-BEC crossover phenomenon[18–20] by controlling the gate voltage of the surface superconductivity. In cold atomic gases, BCS-BEC crossover is seen by tuning the interaction via a Feshbach resonance.[21,22] BCS-BEC crossover in a multiband superconductor was suggested by an ARPES experiment in $FeSe_xTe_{1-x}$.[23] The same situation appears in the surface superconductivity. In Fig. 2(a), the superconducting gap in the fifth sub-band opens at the bottom of the band dispersion. That is, since the gap amplitude $|\Delta|$ is higher than the Fermi energy E_F ($\equiv \mu - E_{l=5,\mathrm{min}}$) from the band bottom, the BEC regime $|\Delta| > E_F$ is realized. The gaps in the other bands, 1–4, are in the BCS regime $|\Delta| < E_F$. As mentioned above, the gap magnitude can be tuned by the gate voltage.

In summary, the local superconducting gap structure and the sub-band dependence in electric-field-induced surface superconductivity were studied by solving the microscopic BdG equation. There, in-gap states appear due to the multiple-gap structure of the multiple-sub-band superconductivity, even for isotropic s-wave pairing. We evaluated how these

structures depend on the screening condition, i.e., triangular potential or self-consistent potential. These characters of the surface superconductivity, due to the sub-band-dependent multigap nature, are important to consider when we discuss the properties of electric-field-induced surface superconductivity.

ACKNOWLEDGMENTS

We thank Professors Y. Iwasa, K. Ueno, and T. Nojima for fruitful discussions and information on their experimental results. This work was supported by KAKENHI Grant No. 21340103.

*ichioka@cc.okayama-u.ac.jp

[1] K. Ueno, S. Nakamura, H. Shimotani, A. Ohtomo, N. Kimura, T. Nojima, H. Aoki, Y. Iwasa, and M. Kawasaki, Nat. Mater. **7**, 855 (2008).

[2] J. T. Ye, S. Inoue, K. Kobayashi, Y. Kasahara, H. T. Yuan, H. Shimotani, and Y. Iwasa, Nat. Mater. **9**, 125 (2011).

[3] K. Ueno, S. Nakamura, H. Shimotani, H. T. Yuan, N. Kimura, T. Nojima, H. Aoki, Y. Iwasa, and M. Kawasaki, Nature Nanotechnol. **6**, 408 (2011).

[4] K. Taniguchi, A. Matsumoto, H. Shimotani, and H. Takagi, Appl. Phys. Lett. **101**, 042603 (2012).

[5] J. T. Ye, Y. J. Zhang, R. Akashi, M. S. Bahramy, R. Arita, and Y. Iwasa, Science **338**, 1193 (2012).

[6] J. Biscaras, N. Bergeal, S. Hurand, C. Grossetête, A. Rastogi, R. C. Budhani, D. LeBoeuf, C. Proust, and J. Lesueur, Phys. Rev. Lett. **108**, 247004 (2012).

[7] J. A. Bert, K. C. Nowack, B. Kalisky, H. Noad, J. R. Kirtley, C. Bell, H. K. Sato, M. Hosoda, Y. Hikita, H. Y. Hwang, and K. A. Moler, Phys. Rev. B **86**, 060503 (2012).

[8] P. G. de Gennes, *Superconductivity of Metals and Alloys* (Addison-Wesley, Reading, MA, 1989).

[9] F. Stern, Phys. Rev. B **12**, 4891 (1972).

[10] T. Ando, A. B. Fowler, and F. Stern, Rev. Mod. Phys. **54**, 437 (1982).

[11] M. Takigawa, M. Ichioka, K. Machida, and M. Sigrist, Phys. Rev. B **65**, 014508 (2001).

[12] M. Takahashi, T. Mizushima, M. Ichioka, and K. Machida, Phys. Rev. Lett. **97**, 180407 (2006).

[13] M. Ichioka and K. Machida, J. Phys. Soc. Jpn. **65**, 4020 (1999).

[14] P. G. de Gennes and D. Saint-James, Phys. Lett. **4**, 151 (1963).

[15] Y. Tanaka, H. Yamagami, and M. Tsukada, Solid State Commun. **79**, 349 (1991).

[16] H. K. Im, E. A. Jagla, and C. A. Balseiro, Phys. Rev. B **50**, 10117 (1994).

[17] S. Kashiwaya and Y. Tanaka, Rep. Prog. Phys. **63**, 1641 (2000).

[18] B. Eagles, Phys. Rev. **186**, 456 (1969).

[19] A. J. Leggett, J. Phys. Colloq. **41**, 7 (1980).

[20] P. Nozieres and S. Schmitt-Rink, J. Low Temp. Phys. **59**, 195 (1985).

[21] M. W. Zwierlein, J. R. Abo-Shaeer, A. Schirotzek, C. H. Schunck, and W. Ketterle, Nature **435**, 1047 (2005).

[22] S. Jochim, M. Bartenstein, A. Altmeyer, G. Hendl, S. Riedl, C. Chin, J. H. Denschlag, and R. Grimm, Science **302**, 2101 (2003).

[23] Y. Lubashevsky, E. Lahoud, K. Chashka, D. Podolsky, and A. Kanigel, Nat. Phys. **8**, 309 (2012).